Nanoscale Advances

PAPER

View Article Online
View Journal | View Issue



Cite this: *Nanoscale Adv.*, 2019, **1**, 4844

# Dye-sensitized $TiO_2$ nanotube membranes act as a visible-light switchable diffusion gate†

Imgon Hwang,[a] Francesca Riboni,[ab] Ekaterina Gongadze,[c] Aleš Iglič,[cd] JeongEun Yoo,[a] Seulgi So,‡[a] Anca Mazare[a] and Patrik Schmuki*[abe]

Received 6th August 2019
Accepted 22nd October 2019

DOI: 10.1039/c9na00480g

rsc.li/nanoscale-advances

Here we report that both-end open anodic $TiO_2$ nanotube membranes, after sensitization with a Ru(II)-based dye, exhibit visible-light switching properties for flow-through the nanotube channels. Under illumination, the gate is in an open state providing ~four-times faster permeation of small molecules through the membrane compared to a dark state. Switching is reversible with no apparent dye degradation being observed. Gating is possible not only of permeating dye molecules but also of nanoprobes such as polystyrene nanospheres. Supported by quantitative modelling, we attribute the switching mechanism to light-induced changes of the charge distribution at the dye/$TiO_2$ interface which in turn alters the hydrodynamics within the anodic tube membranes. This demonstrates that these simple dye-sensitized nanotube membranes can be used as an optically addressable flow-through gate in nanofluidics.



## Introduction

Gating of nanoscale flow-through devices has received major attention in the field of system engineering for controlled "diffusion" applications, for example in drug-delivery, bio-separation, and sensing applications.[1–5] It is important in such devices that nanochannels are reversibly gated, *i.e.*, they can be switched between an open ("on") and closed ("off") state in response to an external stimulus (*e.g.* voltage, pH, or temperature variation).[6–10]

Stimuli-responsive membranes (SRMs) are based on hydrogels,[11] ion-track polymers,[8,10,12] and inorganic solid-state nanochannels such as anodic alumina and silica[7,9,13,14] and the latter can be conveniently modified to exhibit an adaptive gating behavior based on surface termination, reconstruction, and/or local molecular rearrangement.[1] Oxide based nanochannels show remarkable intrinsic robustness and stability, along with an easy chemistry governing channel functionalization for implementing diffusion-gating characteristics *i.e.*, self-assembly or anchoring of (mono)layers of a stimuli-responsive material on the oxide nanochannel surface.[1] Using this approach, diffusion gates based *e.g.* on charge exclusion, hydrophobicity/hydrophilicity switching, and size-selectivity have been explored for ionic current control, molecular separation, and protein fractioning.[7,9,13–16]

The most convenient "wireless" approach to trigger switching in flow-through membranes is the use of light as an on–off switching input. Up to now this is mostly achieved by grafting photo-responsive organic moieties onto the walls of the nanochannels, and the switching is induced by light induced conformational change of the molecule attached to the wall, which in turn affects the permeability properties of the membrane (*e.g.*, wettability, hydrophilicity/hydrophobicity, hydrodynamic diameter, *etc.*).[13,15,17,18]

Here we show that one of the most explored dye sensitized oxides – $TiO_2$ – can effectively be used for visible light flux gating if fabricated as both-end open sensitized membranes. $TiO_2$ nanotube (NT) membranes can be fabricated by combining (i) self-organizing electrochemical anodization to produce one-dimensional $TiO_2$ nanotubes (NTs) on a Ti substrate,[19–21] with (ii) a lift-off process, and this results in self-standing, both-end-open and highly aligned nanochannel/nanotube arrays.[22–25]

Such $TiO_2$ nanotube layers have been recently used as flow-through membranes for the size-selective separation of different solutes, including *e.g.* biologically relevant molecular substrates and micro- and nano-spheres.[26–30]

In the present work, we dye-sensitized $TiO_2$ NT membranes with N719 molecular dye ($[Ru^{II}$(2,2′-bipyridyl-4,4′-dicarboxylate)-$(NCS)_2]TBA_2$, TBA = tetra-*n*-butylammonium), a dye that

[a]*Department of Materials Science WW4-LKO, University of Erlangen-Nuremberg, Martensstrasse 7, 91058 Erlangen, Germany. E-mail: schmuki@ww.uni-erlangen.de*
[b]*Regional Centre of Advanced Technologies and Materials, Šlechtitelů 27, 78371 Olomouc, Czech Republic*
[c]*Laboratory of Biophysics, Faculty of Electrical Engineering, University of Ljubljana, Tržaška 25, SI-1000 Ljubljana, Slovenia*
[d]*Laboratory of Clinical Biophysics, Faculty of Medicine, University of Ljubljana, Zaloška 9, SI-1000 Ljubljana, Slovenia*
[e]*Department of Chemistry, Faculty of Science, King Abdulaziz University, P. O. Box 80203, Jeddah 21569, Saudi Arabia*

† Electronic supplementary information (ESI) available. See DOI: 10.1039/c9na00480g

‡ Current address: POSCO Technical Research Laboratories, Automotive Steel Surface Research Group.

is most commonly used in dye sensitized solar cells (DSSCs). We find that such membranes show visible light-gating effects for *trans*-membrane transport. Supported by quantitative modelling, we show that light-induced perturbation of the electric properties and surface charge of N719/$TiO_2$ tubes affects the tube hydrodynamic properties, and thus can alter the permeation of molecules or nanoscale objects such as polystyrene beads (20 nm). These dye sensitized/$TiO_2$ NT membranes exhibit periodically reversible, visible light-modulated gating characteristics in repetitive light ON–OFF cycles.

# Experimental

### Fabrication of $TiO_2$ nanotube membranes

For anodic nanotube growth, Ti sheets with a thickness of 0.125 mm (99.6% purity, Advent Materials, UK) were used. Prior to anodization, Ti foil was cleaned in acetone, ethanol, and distilled water in an ultrasonic bath and then dried in a $N_2$ stream.

Anodization was carried out in a two-electrode electrochemical cell, with Ti and Pt foils as working and counter electrodes, respectively. An ethylene glycol (EG, 99.5% Sigma-Aldrich) based electrolyte was used that also contained 1.5 M lactic acid (LA, 89% Sigma-Aldrich), 0.1 M ammonium fluoride ($NH_4F$, 98% Sigma-Aldrich) and 5 wt% distilled water.[31] Anodization was carried out at 120 V (Jaissle IMP88 PC) for 10 min. The nanotube layers were then annealed in air at 250 °C for 1 h (heating/cooling rate, 30 °C $min^{-1}$) using a rapid thermal annealer (Jipelec JETFIRST 100 RTA). A second anodization was carried out at 120 V and 60 °C (the temperature was fixed using a thermostat, HAAKE F3) for 3 min to produce a thin underlayer of amorphous $TiO_2$ NTs. This amorphous layer could then selectively be dissolved by dipping the NT films in a 30 wt% $H_2O_2$ aqueous solution for 90 min at room temperature, resulting in the detachment of the upper layer (that is, the tube layer annealed at 250 °C) in the form of a free-standing $TiO_2$ nanotube membrane.

In order to convert the $TiO_2$ nanotubes to anatase, membranes were annealed for 1 h in air at 450 °C (heating/cooling rate, 30 °C $min^{-1}$) using a rapid thermal annealer (Jipelec JETFIRST 100 RTA).

### Materials physico-chemical characterization

Morphological characterization of the nanotubes was carried out with a field-emission scanning electron microscope (FE-SEM, Hitachi S4800). In particular, the NT thickness was measured from the cross sectional SEM images.

The crystallographic properties of the materials were analyzed by X-ray diffraction (XRD) performed with an X'pert Philips MPD (equipped with a Panalytical X'celerator detector) using graphite monochromatic Cu K$\alpha$ radiation ($\lambda = 1.54056$ Å). XRD patterns were collected by placing the membranes on a quartz glass slide. XPS measurements were performed by using X-ray photoelectron spectroscopy (XPS, PHI 5600, US) and peaks were shifted to Ti 2p 458.5 eV.

### Light-modulated gating tests

The functionality of the tube membranes was investigated for the (photo-mediated) transport of the N719 Ru(II) dye ([$Ru^{II}$(2,2′-bipyridyl-4,4′-dicarboxylate)-$(NCS)_2$]$TBA_2$). For this, $TiO_2$ NT membranes were mounted in a PVC holder (with a 0.53 cm-diameter opening) that was used to separate the two compartments (A and B) of a cell. One cell (B) wall was equipped with a quartz glass window.[24,29]

Each compartment was filled with a fixed amount (6 mL) of two different solutions. In detail, a 1.5 mM solution of N719 was prepared in a 1 : 1 acetonitrile/*t*-BuOH mixture; chamber A was then filled with 20 v/v% of the dye solution in EtOH, in order to attain an initial dye concentration of ~300 μM. Chamber B was filled with a 1 : 1 *t*-BuOH/EtOH mixture. The (light-modulated) diffusion of N719 through the NT membrane was monitored on both sides of the cell by measuring the decrease (in chamber A) and increase (in chamber B) of the intensity of the dye main absorption band ($\lambda = 534$ nm) by means of a spectrophotometer (Lambda Bio XLS, PerkinElmer); the dye concentration was afterwards calculated by applying the Beer–Lambert law.[32] A 532 nm LED light (150 mW $cm^{-2}$) was used as the irradiation source, and both the dark and visible light-modulated experiments lasted 8 h.

$AgNO_3$ (1 mM) was added to the dye solution (chamber A) to evaluate the effect of an electron scavenger on the (light-modulated) diffusion of N719 through the tubes. Finally, the membrane functionality was also evaluated for the (light-modulated) permeability of 20 nm polystyrene beads, functionalized with sulfate groups (FluoSpheres® Sulfate Microspheres, 505/515, 2% solids), thus being negatively charged.[33] For this, a specific amount of sulfate microspheres was added to the N719 solution in chamber A to achieve an initial microsphere concentration of ~0.2 mM. The diffusion of the nanospheres through the NT membrane was monitored in both cell compartments by measuring the decrease (A) and increase (B) in the intensity of the microsphere main absorption band ($\lambda =$ *ca.* 500 nm) by means of a spectrophotometer (Lambda Bio XLS, PerkinElmer).

In order to exclude all the possible contributions of dye and/or nanosphere diffusion to the overall kinetics of the different experiments, two sets of control experiments were also performed using $TiO_2$ NT arrays (that is, anchored on Ti foil) and in a more conventional (photo)reactor configuration.[34] In particular, a first set of experiments was performed in the presence of the dye (*t*-BuOH/acetonitrile/ethanol) solution, with and without $Ag^+$, and in the dark or under 532 nm illumination. For a second set of experiments, Ag ions were replaced by the most classic $I^-/I_2$ redox couple for DSSCs.

### Calculations of the spatial dependence of electric potential and electric field strength in the N719 electrolyte solution in contact with a $TiO_2$ surface

The spatial distributions of electric potential and electric field strength were calculated for an ethanol solution of the dissociated Ru(II)-based N719 dye in contact with a $TiO_2$ surface.[35]

In bulk ethanol solution, N719 dissociates into its anionic part ($N719^{2-}$ – for the sake of ease, N719) with a net $-2e_0$ charge ($e_0$ being the unit charge) and two cations $[N(n\text{-}Bu)_4]^+$ ($TBA^+$ – for the sake of ease, TBA), each with a net $+e_0$ charge. The charge of the $TiO_2$ surface is described by its surface charge density, $\sigma_0$.

It is typically reported that N719 anions anchor on the $TiO_2$ surface through carboxylate functional groups. Therefore, owing to a $d_{N719}$ of $\sim 1.5$ nm,[36] we assume a distance of closest approach, for both free N719 anions and TBA cations ($d_{TBA} = ca.$ 1 nm) from the $TiO_2$ surface, equal to $b_2 = 1.5$ nm. Under these conditions, $b_1$ represents the distance between the center of the chemisorbed N719 dye and the $TiO_2$ surface, *i.e.*, $b_1 = 0.75$ nm. Finally, the surface charge density $\sigma_1$ describes the plane charge distribution at a distance $b_1$ from the $TiO_2$ surface.

Taking into account the finite and asymmetric size of ions, the expressions for the spatial distribution of TBA cations ($n_+(x)$), N719 anions ($n_-(x)$) and ethanol ($n_e(x)$) in the electric double layer near a charged $TiO_2$ surface[37] can be derived by using the method of lattice statistics with Boltzmann correction factors[30] which was proven to be equivalent to the method of minimization of the free energy of the system.[37] In the following, $\alpha_+$ and $\alpha_-$ are the number of lattice sites occupied by a single positive and negative ion, respectively, while a single solvent (ethanol) molecule occupies just one lattice site. Considering $d_{TBA} \sim 0.95$ nm,[30] $d_{N719} \sim 1.5$ nm,[36] and $d_{ethanol} \sim 0.46$ nm,[37] we assume $\alpha_+ \approx 3$ and $\alpha_- \approx 13$ and the bulk number density of lattice sites $n_s/N_A = 17.36$ mol $L^{-1}$.

The number densities $n_+(x)$, $n_-(x)$ and $n_e(x)$ can be derived by calculating the corresponding probabilities that a single lattice site in the bulk solution is occupied by one of the three particles (*i.e.* cations, anions or ethanol molecules):

$$n_+(x) = n_s \frac{2n_0\, e^{-e_0\Phi\beta}}{M(\Phi)} \quad (1)$$

$$n_-(x) = n_s \frac{n_0\, e^{+2e_0\Phi\beta}}{M(\Phi)} \quad (2)$$

corrected by the corresponding Boltzmann factors,[37,38] with

$$M(\Phi) = \alpha_+ 2n_0\, e^{-e_0\Phi\beta} + \alpha_- n_0\, e^{+2e_0\Phi\beta} + n_{0e} \quad (3)$$

here $\beta = 1/kT$, where $k$ is the Boltzmann constant, $T$ is the absolute temperature, $n_s$ is the number density of lattice sites, $n_0$ is the bulk number density of anions and cations, $x$ is the distance from the $TiO_2$ surface, $n_{0e}$ is the bulk number density of the solvent (ethanol) and $\Phi$ is the electric potential. In the bulk:

$$n_s = \alpha_+ 2n_0 + \alpha_- n_0 + n_{0e} \quad (4)$$

therefore

$$n_{0e} = n_s - \alpha_+ 2n_0 - \alpha_- n_0.$$

The macroscopic volume charge density in the solution for $x \geq b_2$ is:

$$\rho(x) = e_0 n_+(x) - 2e_0 n_-(x) = -2e_0 n_s n_0 [e^{2e_0\phi\beta} - e^{-e_0\phi\beta}]/M(\Phi) \quad (5)$$

The corresponding Poisson's equation (*i.e.* modified Eigen–Wicke[45] equation) is therefore:

$$\varepsilon_0\varepsilon_r \frac{d^2\phi}{dx^2} = \begin{cases} 0, & 0 \leq x < b_2 \\ 2e_0 n_s n_0 \left[e^{2e_0\phi\beta} - e^{-e_0\phi\beta}\right]/M(\Phi), & x \geq b_2 \end{cases} \quad (6)$$

within appropriate boundary conditions for $\phi$ and $\frac{d\phi}{dx}$ at $x = 0$, $x = b_1$ and $x = b_2$:

$$\frac{d\phi}{dx}(x = 0) = -\frac{\sigma_1}{\varepsilon_0\varepsilon_r} \quad (7)$$

$$\frac{d\phi}{dx}(x = b_{1-}) = \frac{d\phi}{dx}(x = b_{1+}) + \frac{\sigma_2}{\varepsilon_0\varepsilon_r} \quad (8)$$

$$\phi(x = b_{1-}) = \phi(x = b_{1+}) \quad (9)$$

$$\frac{d\phi}{dx}(x = b_{2-}) = \frac{d\phi}{dx}(x = b_{2+}) \quad (10)$$

$$\phi(x = b_{2-}) = \phi(x = b_{2+}) \quad (11)$$

All the above equations are based on the electroneutrality in the bulk solution, where $\frac{d\phi}{dx} = 0$ and $\phi$ assumes a constant value (zero, in our case). The electroneutrality of the system is described by the boundary condition in eqn (7), that is, for $\frac{d\phi}{dx}$ at $x = 0$. Other parameter values are $\sigma_0 = -0.05$ A s $m^{-2}$,[39] relative permittivity $\varepsilon_r = 25$,[40] and absolute temperature $T = 293$ K.

The differential eqn (2), subjected to the boundary conditions (eqn (7)–(11)), was solved numerically using COMSOL 5.3.

## Results and discussion

### $TiO_2$ nanotube membranes

Fig. 1(a) illustrates the experimental procedure for the fabrication of self-standing membranes of vertically aligned $TiO_2$ nanotubes. The as-fabricated membranes (1 cm diameter) are robust, mechanically stable (Fig. 1(b)), and can easily be handled with tweezers; in addition, no serious cracking or damage was observed prior to or after dipping in the N719 dye-based solution or after extended permeation experiments. The membranes (~80–100 nm nanotube diameter) were fabricated using an optimized sequence of double-anodization and mild annealing steps, followed by lift-off from the Ti metal substrate by a chemical etching step (see the ESI for details†).[24,25,41,42]

The etching step not only leads to the complete dissolution of the lower anodic tube layer, but also to that of the bottom of the upper layer, thus resulting in the flow-through nanochannel morphology. Despite the number of steps involved, this sequence leads to self-standing and crack-free tubular layers (Fig. 1(c–e)). The as-formed anodic $TiO_2$ nanotube layers are usually amorphous, and as expected, for the as-synthesized NT layer before chemical etching, only reflections from the underneath Ti foil could be detected, while the tube membrane (that is, detached from the metal substrate and transferred onto a quartz glass) exhibits no specific features, *i.e.*, neither crystalline $TiO_2$ nor Ti reflections could be observed (in line with the

 

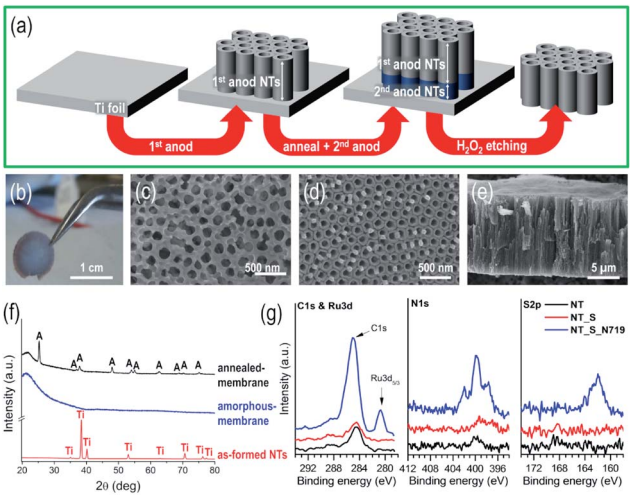


Fig. 1 (a) Schematic of the fabrication of self-standing $TiO_2$ nanotube membranes through a sequence of anodization (anod) steps, annealing and etching. The optical image in (b) shows a robust $TiO_2$ nanotube membrane that could be held with tweezers. (c–e) Top, bottom, and cross-sectional SEM views of the $TiO_2$ NT layer after $H_2O_2$ treatment for the formation of self-standing nanochannel membranes. (f) XRD patterns of (i) $TiO_2$ NTs before detachment from the Ti substrate (red plot), (ii) amorphous self-standing $TiO_2$ tube membrane (blue plot) and (iii) air-annealed (450 °C – 1 h) self-standing $TiO_2$ tube membrane (black plot). XRD patterns of tube membranes were collected by transferring the layer onto a quartz glass. (g) High resolution XPS graphs of C 1s and Ru 3d, and N 1s and O 1s for bare nanotubes (NTs), nanotubes immersed in solution without the dye (NT_S) and nanotubes immersed in the dye solution (NT_S_N719).

amorphous nature of the original tube layer), as shown in Fig. 1(f). Annealing the membrane in air at 450 °C converted $TiO_2$ from amorphous to crystalline anatase; to note, in the absence of the Ti foil underneath, the formation of the undesired rutile phase at the metal/oxide interface is also prevented (this occurs due to the thermal oxidation of metallic Ti).[24,43]

To evaluate the binding of the N719 molecular dye, we immersed the as-synthesized NT layers in the N719 dye solution used during the flow through experiments, *i.e.* a solution containing N719, acetonitrile, *t*-BuOH and EtOH – see Experimental. As a reference, we used a bare NT layer and additionally a NT layer immersed in a solvent solution without N719, NT_S (to account for the possible organics adsorption). The high resolution spectra of the three samples are shown in Fig. 1(g) for C 1s and Ru 3d peaks, N 1s and S 2p; we clearly observe no adsorption from the solvents used in the solution and a clear indication of N719 adsorption due to the increase in C 1s signals, and the appearance of peaks corresponding to Ru $3d_{5/3}$, N 1s and S 2p. First, the C 1s and Ru 3d peaks have a strong overlap; however the Ru $3d_{5/3}$ peak is visible at 280.8 eV (corresponding to $Ru^{II}$),[44,45] while only the Ru $3d_{3/2}$ peak is hidden in the C 1s peaks (peak splitting of Ru 3d is at 4.2 eV and that of Ru $3d_{3/2}$ is at ~285 eV). Thus the C 1s peak evident for the N719 nanotube sample (NT_S_N719) actually shows contributions from C=C, C–C, C–O, C=N (from the NCS groups), TBA groups and Ru $3d_{3/2}$, with small contributions from C–C, C–O and COOH adsorbed on the $TiO_2$ nanotubes[38] (as seen from the small C 1s peaks of NT and NT_S). The N 1s and S 2p spectra confirm dye adsorption due to the presence of N 1s (very low N pickup from the environment for bare nanotubes) and S 2p peaks and these are attributed to the NCS groups (plus the C=N bonds in the pyridine rings, in the case of N1s). The Ti 2p and O 1s peaks are listed in Fig. S1,† and while we observe no difference for the Ti 2p peaks, in the case of O 1s peaks for the N719 nanotube sample, we observe a broadening of the O peak towards higher binding energies which is correlated with the CO and COOH groups of the dye.

## Visible light-responsive diffusion gate

The as-fabricated N719/$TiO_2$ NT membranes are active in the visible spectral region where $TiO_2$ is transparent and photoinert ($E_{g,TiO_2} \sim 3.2$ eV).[46] The functionality of these highly defined, robust and crystalline $TiO_2$ NT membranes was tested in a flow-through configuration for gated ion-diffusion, namely for (photo-assisted) diffusion experiments with the membranes sandwiched as a separator in the two-compartment cell, as shown in Fig. 2(a). The two sides of the cell were filled with a 20 v/v% N719 solution in EtOH (see details in Experimental), and with an EtOH based "reference solution"; before diffusion, the solution in compartment A exhibits a dark orange color owing to the Ru(II)-based dye, while the dye-free solution in compartment B is transparent and colorless. The temperature increase in both cell compartments during the illumination experiments is small (*e.g.* for 8 h illumination, the temperature increase was 3 °C, from 23.8 to 27 °C).

We first tested the permeability of the NT membrane to N719 molecules in the dark by measuring the dye concentration in both cell compartments and as anticipated, the N719 molecules diffuse through the membrane from the higher dye concentration side (A) to the lower one (B), until an equilibrium state is achieved, after *ca.* 7 hours, as discussed in the ESI and Fig. S2(a–d).† The concentration gradient ($\Delta C$) across the tube membrane is the driving force and assuming a first-order kinetics for dye diffusion, a linear dependence of $\ln(\Delta C/C_{tot})$ *vs.* time is observed (Fig. 2(b)), with $k_{dark} = 8.5 \times 10^{-2}$ $h^{-1}$. A N719 diffusion coefficient $D$ of $\sim 10^{-7}$ $cm^2$ $s^{-1}$ was extracted using a classic Fick approach[47] – this is in line with previous reports on dye permeability through an anodic flow-through tube membrane.[24,27] The value therefore confirms the absence of cracks or leaks within the membrane.

To note, the dye becomes partially adsorbed on the $TiO_2$ tube membrane during flow through, and even if a significant change of the membrane color is also observed after 8 h of immersion in the N719 solution; however the total amount of free N719 in solution was not significantly affected by the amount adsorbed on the tubes. This, as the total dye concentration (measured in both cells), remains constant over the whole time range of the flow through experiments (middle panel, Fig. S2(a)).†

When the system is irradiated with a 532 nm-LED light, the diffusion of N719 molecules through the $TiO_2$ nanotube membrane becomes significantly affected, as under illumination, the decrease/increase of the N719 amount on both sides of

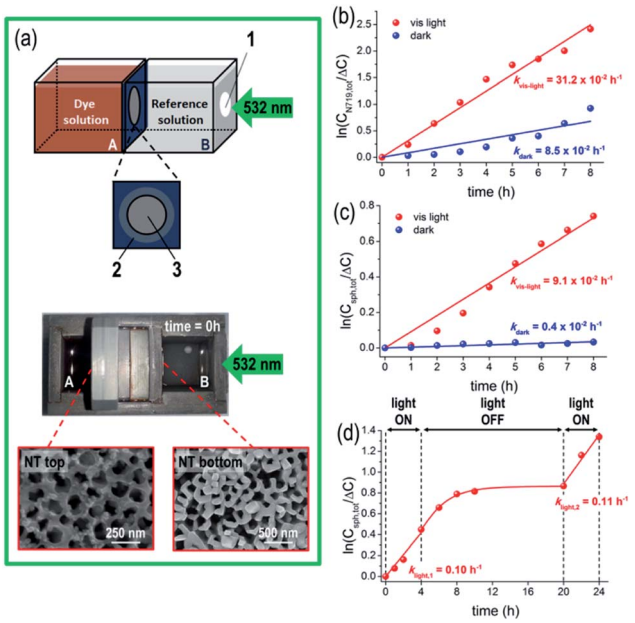


Fig. 2 (a) Upper panel shows the sketch of the setup used for flow-through photocatalytic experiments. Chamber A contains 20 v/v% dye solution in ethanol (dye solution: 300 μM N719 in 1 : 1 acetonitrile/*tert*-butanol mixture) – for the polystyrene nanosphere experiments, the required amount of nanoparticles was also added in order to attain 200 μM initial concentration; chamber B contains the blank reference solution (1 : 1 *tert*-butanol/ethanol mixture). 1 represents the quartz glass window for 532 nm illumination, 2 indicates the entire tube membrane ($d$ = 1 cm) and 3 is the actual membrane surface exposed to solutions and light ($d$ = 0.53 cm). Lower panel shows the optical image of the two-compartment reactor before the diffusion experiment starts ($t$ = 0 h), filled-in with the dye (A) and blank background (B) solutions. The SEM images show the top and bottom of a tube membrane. The membrane was always mounted with the tube top facing the dye solution and the tube bottom facing the reference solution. Kinetics of the dye (b) and nanosphere (c) flow across a tube membrane, in the dark and under 532 nm illumination. A first order rate law, that is, linear dependence of $\ln(C_{tot}/\Delta C)$ *vs.* time, is assumed. (d) Kinetics of nanosphere separation through a dye pre-sensitized tube membrane, in light ON–OFF cycles.

the cell is faster than that in the absence of light (red plots in Fig. S3(a)).† From the quantitative data, a *ca.* 4-times larger kinetic constant was calculated for the light-driven diffusion (*i.e.*, $k_{light} = 31.2 \times 10^{-2}$ h$^{-1}$, see Fig. 2(b)), confirming the first-order kinetics of the reaction, resulting in a higher N719 diffusion coefficient $D$ of $\sim 4 \times 10^{-7}$ cm$^2$ s$^{-1}$.

Regarding the photo-induced degradation of the dye, when $Ag^+$ ions are present in the diffusing electrolyte no significant dye degradation is observed (that is, the total N719 concentration remains constant over time, lower panel in Fig. S2(a)).† We attribute this effect of $Ag^+$ ions to their electron-scavenging properties and their ability of coordinating (free) –NCS ligands of the Ru(II)-based dye. In general, dye photo-degradation can be prevented if the composition of the diffusing medium contains a suitable electron scavenging species (see also Fig. S3 and the ESI for discussion†).

Based on the above data, the dye/$TiO_2$ NT membranes behave as smart nanofluidic systems with visible light-tunable hydrodynamic and permeability properties[29] (*i.e.*, $k_{light}/k_{dark}$ = *ca.* 4). Supported by theoretical modeling (see below), we show that this effect can be ascribed to a light-promoted perturbation of the dye/tube electric properties upon electron injection from N719 (adsorbed on the tube walls) to $TiO_2$ (*i.e.*, in line with the principles reported for DSSCs[48,49]).

The full visible light-responsive on/off gating functionality of a dye-sensitized $TiO_2$ flow-through membrane was then explored for the diffusion of an inert nanoprobe, that is, 20 nm diameter spherical, fluorescence labeled polystyrene nanoparticles (NPs or nanospheres).[33] Nanosphere diffusion through the tube membrane was followed by UV-vis absorption spectroscopy in both chambers of the reactor, by measuring the change in the intensity of the nanosphere label with a maximum absorption band at $\lambda$ = *ca.* 500 nm. The N719/$TiO_2$ NT membrane behaves also in this case as a photo-switchable diffusion gate (Fig. S4(a)),† that is, NP diffusion is almost fully prevented in the dark, but it occurs when the system is under 532 nm illumination. In other words, the membrane switches from a (apparent) closed state in the absence of light to a gate-open state under 532 nm light.

Assuming a first-order kinetic dependence of the nanosphere concentration *vs.* time (Fig. 2(c)), the rate constants for the dark and light processes indicate a significantly faster nanosphere flux across the tube membrane under light than in the dark ($k_{light}/k_{dark}$ = *ca.* 23). Similarly, we observed that nanospheres adsorb to a small extent on the NT tops, as seen in the SEM images of the tube top and bottom of a membrane after the experiment (Fig. 2(a)). However, the total amount of nanospheres (determined on both sides of the reactor) remains constant over the investigated time (middle and lower panels in Fig. S4(a));† thus no (photo-)degradation and/or significant adsorption on the tube wall occurs that would affect the experiment.

Excluding any clogging of the tube membrane by nanospheres (the tube diameter is ~80–100 nm *vs.* the NPs diameter ~20 nm), the slower NP *trans*-membrane permeation observed in the dark compared with the N719 dye is approximately in line with the Stokes–Einstein relation, where $D$ is inversely proportional to the radius ($r$) of the diffusing species, that is, $D \propto r^{-1}$.[50] Therefore, the diffusion coefficient of 20 nm diameter nanospheres ($r$ = 10 nm) is expected to be more than 10 times smaller than that of N719 molecules ($r_{N719} \sim 0.8$ nm [36]).[27]

However, it is evident from Fig. 2(c) (red plot) that the flux of NPs through the NT membrane becomes significantly enhanced when the system is irradiated with the 532 nm LED. In line with the results of dye ion-mobility, we attribute this effect to the light-mediated nanofluidics of the dye/$TiO_2$ flow-through membrane due to the perturbation of the electrical and hydrodynamic properties which follows electron injection from the photo-excited dye into $TiO_2$. Furthermore, in the absence of a light-responsive molecule (*i.e.* no dye adsorbed on the tube walls) the $TiO_2$ tube membrane maintains a "*closed*" state that prevents polystyrene nanosphere diffusion (see below and the ESI, Fig. S5†).

These experiments show that the modulation of the nanofluidic gating properties of flow-through sensitized $TiO_2$ tube

membranes is valid regardless of the nature (*i.e.*, light-responsive *vs.* light-inert) and size (*i.e.*, 1.5 nm *vs.* 20 nm) of the diffusing species, indicating the underlying mechanism to be the same and to originate from the dye-sensitized tube walls.

Fig. 2(d) shows the results for the nanosphere diffusion using a dye-sensitized tube membrane in repetitive light ON–OFF cycles. During the initial light-ON period, diffusion of nanospheres through the membrane is observed, namely the membrane is in an open state providing fast NP diffusion. A kinetic constant $k_{light,1} = 0.10\ h^{-1}$ in line with that measured for the system with free dye molecules in the diffusing medium (Fig. 2(c)) confirms that a plain dye-sensitized membrane can deliver a similar light-regulated diffusion efficiency – *i.e.*, no excess of free dye molecules in the diffusing medium is required. When the light is turned off, a slow decay of NP diffusion is observed (that is, switching of the sensitized tube membrane diffusion properties occurs on a longer time scale), followed by a significant drop in the kinetics of NP flow-through, *i.e.*, the membrane is switched to a "gate-off" state. The permeability characteristics could be fully restored when the 532 nm LED light was turned on again, namely when the photo-promoted electron (from N719) mediated process was re-activated and the membrane switched back to a "gate-on" state for NP diffusion. We did not observe a decay of the activity of the membranes during several days and in addition, switching is reversible with no apparent dye degradation (to note, there is no photo-induced degradation of the N719 dye in the solution in the presence of $Ag^+$ ions). This, as a comparison of the kinetic constants of the light-ON periods, with $k_{light,1} \sim k_{light,2}$, is in line with the reversible gate on/off characteristics of a dye-sensitized tube membrane, and also confirms the long-term stability of this approach for fabricating light-responsive flow-through systems.

## Modelling

In order to assess the causes of the effect, we modelled the investigated dye/$TiO_2$ NT system according to the schemes in Fig. 3. A key consideration is to simulate the effects produced under irradiation on the tube electric potential and electric field as a function of the distance from the tube surface ($x$).

In solution, N719 typically dissociates into two tetrabutylammonium cations (TBA), each holding a positive charge $+e_0$, and a Ru(II)-based molecular complex, the "dye", that features two negative charges ($-2e_0$) localized on $-COO^-$ groups.

N719 anions adsorb on the $TiO_2$ surface through carboxylate binding/interaction *e.g.*, with under-coordinated Ti surface sites, *via* hydrogen bonding or van der Waals interactions[51,52] – typically, the adsorption mode of carboxylic groups on $TiO_2$ is crucial to enable efficient charge transfer from the dye donor group to the semiconductor.[53]

For $TiO_2$ nanotubes, we recently showed that the adsorption/binding efficiency of a molecule is surface curvature-dependent and that at highly curved rims (*i.e.*, tube tops) is maximized due to a maximum of the $TiO_2$ surface charge density ($\sigma$).[37,38,54] Based on these and previous findings that showed that the surface of 20 nm diameter $TiO_2$ nanoparticles (*i.e.*, NPs with a highly curved surface) is uniformly covered by a N719-based monolayer,[55] we assume that the (sharp edges of) tube walls (either at NT tops or bottoms) and the NT surfaces are decorated uniformly with N719 molecules (see models in Fig. 3).

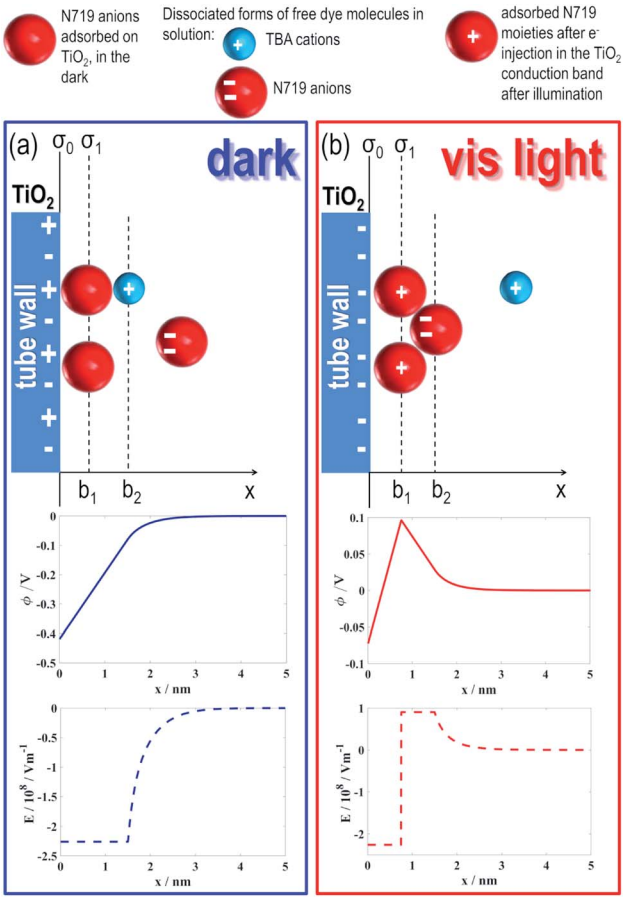


Fig. 3 (a and b) represent the dye/$TiO_2$ tube system at equilibrium (under dark) and under 532 nm illumination, respectively. In particular, the upper panels represent the model used for calculating the spatial distributions of the electric potential ($\phi$, middle panels) and the electric field strength ($E$, lower panels) as a function of the distance from the surface of a $TiO_2$ tube ($x$). Positive charges on the $TiO_2$ surface in the dark represent under-coordinated Ti surface sites where N719 anions likely adsorb, thus becoming electrically neutral. Red spheres, with two negative charges ($-2e_0$), and light blue spheres, with a positive charge ($+e_0$), represent the dissociated form of free dye molecules in the diffusing medium, that is, N719 anions and TBA cations, respectively. Red spheres, with a positive charge ($+e_0$), represent adsorbed N719 moieties after electron injection into the $TiO_2$ conduction band upon illumination (*i.e.*, Ru(III)). $\phi(x)$ and $E(x)$ were calculated by quantitatively solving the modified Wicke–Eigen equation, with $\alpha_+ = 3$, $\alpha_- = 13$, $n_s/N_A = 17.36$ mol $L^{-1}$ and $n_0/N_A = 0.06$ mol $L^{-1}$ and room temperature, subjected to appropriate boundary conditions (for details, see Experimental).

To estimate the space dependence of the electric potential ($\phi$) and the corresponding electric field strength ($E$) in the vicinity of the dye-decorated $TiO_2$ surface (before and after light irradiation), we quantitatively solved the modified Wicke–Eigen equation (for derivation and definitions of the symbols, see Experimental and the two upper panels in Fig. 3):

$$\varepsilon_0\varepsilon_r\nabla^2\phi = \frac{2e_0n_sn_0[e^{2e_0\phi\beta} - e^{-e_0\phi\beta}]}{\alpha_+2n_0\ e^{-e_0\Phi\beta} + \alpha_-n_0\ e^{+2e_0\Phi\beta} + n_{0e}} \quad (12)$$

within appropriate boundary conditions, as from our model of the $TiO_2$ surface represented in Fig. 3. The applied force ($F_{dye}$) on the negatively charged N719 free dye molecules ($-2e_0$) at a specific distance ($x$) from the $TiO_2$ surface is then calculated as $F_{dye}(x) = -2e_0E(x)$, and the extracted values are reported in Table 1.

At equilibrium, *i.e.* when no light is provided (Fig. 3(a)), N719 adsorbed on the $TiO_2$ surface "shares" (a fraction of) the initial $-2e_0$ charge with $TiO_2$ and, in line with this, a negative electric potential ($\Phi < 0$) region (middle panel, Fig. 3(a)) and a corresponding negative electric field ($E < 0$) region (lower panel, Fig. 3(a)) were found to extend to a minimum of 1.5 nm (*i.e.*, the diameter of a N719 molecule[36]) from the $TiO_2$ surface (see Experimental for calculation details). This leads to a (electrostatic) repulsion (see the first column in Table 1) between the $TiO_2$ surface covered by adsorbed dye molecules (Fig. 3(a)) and free anions in solution and therefore to hindered access to the free anions in the tube membrane, resulting consequently in a slow flow-through diffusion kinetics. These simulated findings are in accordance with our experimental results (Fig. 2(b)).

However, under light irradiation (Fig. 3(b)), that is, when N719 is photo-excited and photo-promoted electrons are injected from the LUMO of the dye into the CB of $TiO_2$, the electric charge situation of the dye/$TiO_2$ system dramatically changes: at a specific distance, $x > b_1$ where $b_1$ corresponds to the radius of N719 (*i.e.*, $b_1 = 0.75$ nm), a positive electric potential and electric field strength occur, as shown in the middle and lower panel, respectively, Fig. 3(b). Namely, the light-promoted $e^-$ injection from the dye creates a negative-charge depleted region in the vicinity of the $TiO_2$ nanotube surface. In addition, a direct consequence of the $e^-$ injection on $TiO_2$ from the photo-excited dye is in fact the oxidation of Ru(II) to Ru(III), that is, the "dye" becomes positively charged (which is well-known for the N719 dye used in dye sensitized solar-cells based on nanostructured $TiO_2$).

Table 1 Calculated force (in pN) applied on the negatively charged free N719 dye molecules at different distances from the $TiO_2$ surface before light irradiation (repulsion force) and after light irradiation (attraction force). Except $n_0/N_A = 0.2$ mmol $L^{-1}$, the values of other model parameters are the same as in Fig. 3

| $x$ (nm) | Repulsion $F^a$ (pN) | Attraction $F^b$ (pN) |
|---|---|---|
| 10 | 72.4 | −28.9 |
| 2 | 23.3 | −10.7 |
| 3 | 9.6 | −4.6 |
| 4 | 6.0 | −2.8 |
| 6 | 3.4 | −1.5 |
| 8 | 2.3 | −1.0 |
| 10 | 1.8 | −0.7 |
| 12 | 1.4 | −0.5 |
| 16 | 1.0 | −0.3 |

[a] Before visible light irradiation. [b] After visible light irradiation.

Therefore, the plane charge density $\sigma_1 = e_0/(d_{N719})^2$ at $b_1$ describing the charge of a photo-oxidized dye layer on $TiO_2$ becomes positive, ~0.07 A s $m^{-2}$ (calculated for $n_0/N_A = 0.06$ mol $L^{-1}$), in contrast to $\sigma_1 = 0$ A s $m^{-2}$ before light irradiation (in the dark, the dye/$TiO_2$ system is indeed considered under an electroneutrality regime).

The positively charged layer of irradiated N719 molecules produces a positive electric field (lower panel, Fig. 3(b)) and a consequent short-range attractive force on the free negatively charged dye molecules in solution (see right column in Table 1). Hence, the access of free dye molecules in the tube membrane is promoted with a direct consequence on the dye *trans*-membrane flow, in accordance with our experimental results (Fig. 2(b)).

In the calculations of attractive and repulsive forces presented in Table 1, a much smaller bulk concentration of ions ($n_0/N_A$) was assumed than that in Fig. 3; therefore the electric double layer also protrudes much deeper into the solution than as shown in Fig. 3. More importantly, the $n_0/N_A$ value of 0.2 mmol $L^{-1}$ used in the calculations presented in Table 1 is in the range of the used experimental value (see for example Fig. S2(a) in the ESI†). Table 1 reveals that the effect of light-induced charge switching extends more than 10 nm away from the inner surface of the $TiO_2$ nanotube. Thus, a 10 nm thick ring on the inner surface of the nanotube presents around 40% of the inner cross sectional area of an 80–100 nm inner diameter nanotube. This affects in this range the hydrodynamic flow of charge (the flux of charged particles) through the tubes. In more detail, the positive charges accumulated on the surface of the tube wall (created by adsorbed N719 moieties after electron injection into the $TiO_2$ conduction band upon illumination) produce a positive electric field and a short-range attractive force that can affect the free N719 anion movement in the solution (diffusion). Therefore, it can be concluded that light-induced charge switching can considerably change the transport through nanotubes, in accordance with experimental observations presented in this work.

We have recently shown that a modification of the electrical properties of a $TiO_2$ tube membrane, induced *e.g.* by adjusting the electrolyte pH and/or composition, affects its surface electrokinetic properties.[29] Based on these findings, we now assume that a similar effect on the hydrodynamics of a dye/tube membrane can also be observed due to a change of its charge surface density promoted by visible light illumination: positive charges accumulated at $x = b_1$ may indeed attract free (negatively charged) N719 ions in solution and boost their diffusion. In line with this, our experimental results show that a ~4-times faster flow-through migration of the dye occurs across the NT membrane under 532 nm light, with respect to diffusion in the dark (*i.e.*, concentration gradient-driven).

This visible-light promoted effect could be exploited and, most remarkably, can be modulated reversibly under light ON–OFF conditions for transporting inert spectator molecules, that is, molecular substrates that are not directly involved in the photopromoted charge distribution switching, as we show *e.g.* for the negatively charged polystyrene nanospheres that undergo a similar gating mechanism.

 

## Conclusions

In the present work, we show that dye sensitized anodic $TiO_2$ nanotube membranes can be exploited as visible light switchable gates. $TiO_2$ NT membranes sensitized with N719 can be stimulated with 532 nm illumination and show an altered flux (diffusion) through the tube membrane of not only dye molecules but also of inert polystyrene nanospheres. This effect can be regulated reversibly in light ON–OFF cycles. We attribute these visible light-adjustable diffusion features to the modification of the dye/$TiO_2$ interface electrical properties which occurs under illumination. The re-arrangement of the electric charge along the walls of the NT membrane is key and affects the hydrodynamic properties within a tube channel and thus the permeability characteristics. These N719/$TiO_2$ tube gated membranes, with a visible-light driven trigger, can be regarded as a new platform to optically control flow-through in nanofluidic devices.

## Conflicts of interest

There are no conflicts to declare.

## Acknowledgements

The authors would like to acknowledge ERC (project ID: 340511), DFG and the DFG "cluster of excellence" EAM (Grant no. EXC 315), and ARRS grant No. P2-0232 for financial support.

## Notes and references

1 M. A. C. Stuart, W. T. S. Huck, J. Genzer, M. Müller, C. Ober, M. Stamm, G. B. Sukhorukov, I. Szleifer, V. V. Tsukruk, M. Urban, E. Winnik, S. Zauscher, I. Luzinov and S. Minko, *Nat. Mater.*, 2010, **9**, 101.
2 A. K. Fard, G. McKay, A. Buenkenhoudt, H. Al Sulaiti, F. Motmans, M. Khraisheh and M. Atieh, *Materials*, 2018, **11**, 74.
3 E. M. Hoek, V. V. Tarabara, K.-H. Wee and R. Bai, Stimuli-Responsive Membranes, in *Encyclopedia of Membrane Science and Technology – Membrane Materials, Characterization and Module Design*, ed. E. M. Hoek and V.V. Tarabara, 2013.
4 R. van den Hurk and S. Evoy, *Sensors*, 2015, **15**, 14045.
5 M. E. Idrissi, C. E. Meyer, L. Zarntner and W. Meier, *J. Nanobiotechnol.*, 2018, **16**, 63.
6 O. Beckstein, P. C. Biggin and M. S. P. Sansom, *J. Phys. Chem. B*, 2000, **105**, 12902.
7 S. Kim, E. I. Ozalp, M. Darwish and J. A. Weldon, *Nanoscale*, 2018, **10**, 20740.
8 M. Ali, P. Ramirez, S. Mafé, R. Neumann and W. Ensinger, *ACS Nano*, 2009, **3**, 603.
9 S. N. Smirnov, I. V. Vlassiouk and N. V. Lavrik, *ACS Nano*, 2011, **5**, 7453.
10 L. J. Small, D. R. Wheeler and E. D. Spoerke, *Nanoscale*, 2015, **7**, 16909.
11 D. J. Beebe, J. S. Moore, J. M. Bauer, Q. Yu, R. H. Liu, C. Devadoss and B.-H. Jo, *Nature*, 2000, **404**, 588.
12 B. Yameen, M. Ali, R. Neumann, W. Ensinger, W. Knoll and O. Azzaroni, *Nano Lett.*, 2009, **9**, 2788.
13 I. Vlassiouk, C.-D. Park, S. A. Vail, D. Gust and S. Smirnov, *Nano Lett.*, 2006, **6**, 1013.
14 Q. Zhang, Z. Zhang, H. Zhou, Z. Xie, L. Wen, Z. Liu, J. Zhai and X. Diao, *Nano Res.*, 2017, **10**, 3715.
15 Q. Zhang, J. Kang, Z. Xie, X. Diao, Z. Liu and J. Zhai, *Adv. Mater.*, 2018, **30**, 1703323.
16 D. G. Haywood, A. Saha-Shah, L. A. Baker and S. C. Jacobson, *Anal. Chem.*, 2015, **87**, 172.
17 N. Liu, D. R. Dunphy, P. Atanassov, S. D. Bunge, Z. Chen, G. P. López, T. J. Boyle and C. Jeffrey Brinker, *Nano Lett.*, 2004, **4**, 551.
18 Q. Q. Zhang, Z. Y. Liu, K. F. Wang and J. Zhai, *Adv. Funct. Mater.*, 2015, **25**, 2091.
19 K. Lee, A. Mazare and P. Schmuki, *Chem. Rev.*, 2014, **114**, 9385.
20 F. Riboni, N. T. Nguyen, S. So and P. Schmuki, *Nanoscale Horiz.*, 2016, **1**, 445.
21 S. Ozkan, A. Mazare and P. Schmuki, *Electrochim. Acta*, 2018, **268**, 435.
22 F. Mohammadpour, M. Moradi, K. Lee, G. Cha, S. So, A. Kahnt, D. Guldi, M. Altomare and P. Schmuki, *Chem. Commun.*, 2015, **51**, 1631.
23 F. Mohammadpour, M. Moradi, G. Cha, S. So, K. Lee, M. Altomare and P. Schmuki, *ChemElectroChem*, 2015, **2**, 204.
24 S. So, I. Hwang, F. Riboni, J. E. Yoo and P. Schmuki, *Electrochem. Commun.*, 2016, **71**, 73.
25 S. So, I. Hwang, S. Mohajernia, M. Mackovic, E. Spiecker, G. Cha, A. Mazare and P. Schmuki, *Adv. Energy Mater.*, 2018, **8**, 1800981.
26 P. Roy, T. Dey, K. Lee, D. Kim, B. Fabry and P. Schmuki, *J. Am. Chem. Soc.*, 2010, **132**, 7893.
27 S. P. Albu, A. Ghicov, S. Berger, H. Jha and P. Schmuki, *Electrochem. Commun.*, 2010, **12**, 1352.
28 J. Xu, L. Yang, Y. Han, Y. Wang, X. Zhou, Z. Gao, Y.-Y. Song and P. Schmuki, *ACS Appl. Mater. Interfaces*, 2016, **8**, 34.
29 S. Mohajernia, A. Mazare, E. Gongadze, V. Kralj-Iglič, A. Iglič and P. Schmuki, *Electrochim. Acta*, 2017, **245**, 25.
30 Z. Dai, L. Yang, Y. Li, C. Zhao, J. Guo, Z. Gao and Y.-Y. Song, *Chem. Commun.*, 2019, **55**, 10571.
31 S. So, K. Lee and P. Schmuki, *J. Am. Chem. Soc.*, 2012, **134**, 11316.
32 M. K. Nazeeruddin, A. Kay, I. Rodicio, R. Humphry-Baker, E. Mueller, P. Liska, N. Vlachopoulos and M. Gratzel, *J. Am. Chem. Soc.*, 1993, **115**, 6382.
33 S. Coertjens, R. De Dier, P. Moldenaers, L. Isa and J. Vermant, *Langmuir*, 2017, **33**, 2689.
34 I. Paramasivam, J. M. Macak and P. Schmuki, *Electrochem. Commun.*, 2008, **10**, 71.
35 S. McLaughlin, *Annu. Rev. Biophys. Biophys. Chem.*, 1989, **18**, 113.
36 P. Marquet, G. Andersson, A. Snedden, L. Kloo and R. Atkin, *Langmuir*, 2010, **26**, 9612.

37 M. Kulkarni, A. Mazare, E. Gongadze, S. Perutkova, V. Kralj-Iglič, I. Milošev, P. Schmuki, A. Iglič and M. Mozetič, *Nanotechnology*, 2015, **26**, 62002.
38 M. Kulkarni, A. Mazare, J. Park, E. Gongadze, M. S. Killian, S. Kralj, K. von der Mark, A. Iglič and P. Schmuki, *Acta Biomater.*, 2016, **45**, 357.
39 M. Lorenzetti, E. Gongadze, M. Kulkarni, I. Junkar and A. Iglič, *Nanoscale Res. Lett.*, 2016, **11**, 378.
40 M. Mohsen-Nia, H. Amiri and B. Jazi, *J. Solution Chem.*, 2010, **39**, 701.
41 J. Choi, S.-H. Park, Y. S. Kwon, J. Lim, I. Y. Song and T. Park, *Chem. Commun.*, 2012, **48**, 8748.
42 G. Cha, P. Schmuki and M. Altomare, *Chem.–Asian J.*, 2016, **11**, 789.
43 K. Zhu, N. R. Neale, A. F. Halverson, J. Y. Kim and A. J. Frank, *J. Phys. Chem. C*, 2010, **114**, 13433.
44 J. Singh, A. Gusain, V. Saxena, A. K. Chauhan, P. Veerender, S. P. Koiry, P. Jha, A. Jain, D. K. Aswal and S. K. Gupta, *J. Phys. Chem. C*, 2013, **117**, 21096.
45 L. M. Martinez-Prieto, S. Carenco, C. H. Wu, E. Bonnefille, S. Axnanda, Z. Liu, P. F. Fazzini, K. Philippot, M. Salmeron and B. Chaudret, *ACS Catal.*, 2014, **4**, 3160.
46 M. Grätzel, *Nature*, 2001, **414**, 338.
47 K. L. Kostka, M. D. Radcliffe and E. J. von Meerwall, *Phys. Chem.*, 1992, **96**, 2289.
48 B. O'Regan and M. Grätzel, *Nature*, 1991, **353**, 737.
49 M. Grätzel, *Inorg. Chem.*, 2005, **44**, 6841.
50 A. Einstein, *Ann. Phys.*, 1905, **322**, 549.
51 K. Kalyanasundaram and M. Grätzel, *Coord. Chem. Rev.*, 1998, **177**, 347.
52 F. De Angelis, S. Fantacci, A. Selloni, M. K. Nazeeruddin and M. Grätzel, *J. Phys. Chem. C*, 2010, **114**, 6054.
53 A. Hagfeldt, G. Boschloo, L. Sun, L. Kloo and H. Pettersson, *Chem. Rev.*, 2010, **110**, 6595.
54 E. Gongadze, D. Kabaso, S. Bauer, T. Slivnik, P. Schmuki, U. van Rienen and A. Iglič, *Int. J. Nanomed.*, 2011, **6**, 1801.
55 R. Katoh, A. Huijser, K. Hara, T. J. Savenije and L. D. A. Siebbeles, *J. Phys. Chem. C*, 2007, **111**, 10741.